BMJ Open Respiratory Research

Time-course transcriptome analysis of a double challenge bleomycin-induced lung fibrosis rat model uncovers ECM homoeostasis-related translationally relevant genes

Martina Bonatti ,[1,2] Vanessa Pitozzi,[3] Paola Caruso,[3] Silvia Pontis,[3] Maria Gloria Pittelli,[3] Caterina Frati,[4] Chiara Mangiaracina,[4] Costanza Anna Maria Lagrasta,[4] Federico Quaini,[4] Simona Cantarella,[1,5] Simone Ottonello,[1] Gino Villetti,[3] Maurizio Civelli,[3] Barbara Montanini ,[1,6] Marcello Trevisani[3]

To cite: Bonatti M, Pitozzi V, Caruso P, *et al*. Time-course transcriptome analysis of a double challenge bleomycin-induced lung fibrosis rat model uncovers ECM homoeostasis-related translationally relevant genes. *BMJ Open Respir Res* 2023;**10**:e001476. doi:10.1136/bmjresp-2022-001476

► Additional supplemental material is published online only. To view, please visit the journal online (http://dx.doi.org/10.1136/bmjresp-2022-001476).

BM and MT are joint senior authors.

Received 28 September 2022
Accepted 30 August 2023

For numbered affiliations see end of article.

Correspondence to
Dr Barbara Montanini; barbara.montanini@unipr.it

ABSTRACT

Background Idiopathic pulmonary fibrosis (IPF) is an irreversible disorder with a poor prognosis. The incomplete understanding of IPF pathogenesis and the lack of accurate animal models is limiting the development of effective treatments. Thus, the selection of clinically relevant animal models endowed with similarities with the human disease in terms of lung anatomy, cell biology, pathways involved and genetics is essential. The bleomycin (BLM) intratracheal murine model is the most commonly used preclinical assay to evaluate new potential therapies for IPF. Here, we present the findings derived from an integrated histomorphometric and transcriptomic analysis to investigate the development of lung fibrosis in a time-course study in a BLM rat model and to evaluate its translational value in relation to IPF.

Methods Rats were intratracheally injected with a double dose of BLM (days 0–4) and sacrificed at days 7, 14, 21, 28 and 56. Histomorphometric analysis of lung fibrosis was performed on left lung sections. Transcriptome profiling by RNAseq was performed on the right lung lobes and results were compared with nine independent human gene-expression IPF studies.

Results The histomorphometric and transcriptomic analyses provided a detailed overview in terms of temporal gene-expression regulation during the establishment and repair of the fibrotic lesions. Moreover, the transcriptomic analysis identified three clusters of differentially coregulated genes whose expression was modulated in a time-dependent manner in response to BLM. One of these clusters, centred on extracellular matrix (ECM)-related process, was significantly correlated with histological parameters and gene sets derived from human IPF studies.

Conclusions The model of lung fibrosis presented in this study lends itself as a valuable tool for preclinical efficacy evaluation of new potential drug candidates. The main finding was the identification of a group of persistently dysregulated genes, mostly related to ECM homoeostasis, which are shared with human IPF.

WHAT IS ALREADY KNOWN ON THIS TOPIC

⇒ Recent progress in preclinical models of pulmonary fibrosis provided valuable insights for study idiopathic pulmonary fibrosis (IPF). Nevertheless, the lack of approved treatments highlights the necessity for multiple well-characterised animal models.

WHAT THIS STUDY ADDS

⇒ The murine bleomycin (BLM) lung fibrosis model, despite not fully resembling the disease, is widely used to study IPF. We extensively examined gene-expression changes during the temporal evolution of lung fibrosis in a specific rat BLM model in comparison with IPF, discovering a common set of dysregulated genes, primarily linked with extracellular matrix (ECM) homoeostasis.

HOW THIS STUDY MIGHT AFFECT RESEARCH, PRACTICE OR POLICY

⇒ The described model and its translationally relevant transcriptional signature could represent a useful tool to evaluate and compare new potential drug candidates acting on critical pathways implicated in IPF development and ECM turnover.

BACKGROUND

Idiopathic pulmonary fibrosis (IPF) is a deadly interstitial lung disease (ILD) of unknown origin that is marked by progressive restrictive-ventilatory limitation, hypoxia, dyspnoea and cough.[1] IPF develops over time as the result of a set of genetic and environmental cues not yet well clarified and characterised by specific hallmarks, such as the usual interstitial pneumonia pattern.[2] Although two approved drugs, pirfenidone and nintedanib, have demonstrated attenuation of IPF

progression and improvement in survival rate,[3–5] still no cure of IPF is available and new treatment strategies are needed.[2]

Success during early drug development and preclinical proof of concept are profoundly dependent on the use of an animal model that can enforce scientific confidence on a specific target, while reliably predicting clinical efficacy of new drug candidates. Although various animal models have been used in recent years, a fully satisfactory preclinical model capable of recapitulating the complex features of human IPF is not yet available.[6] Indeed, according to a recent report from the Official American Thoracic Society Workshop,[6] the bleomycin (BLM) murine model is still considered the best-characterised animal model available for preclinical testing in IPF.[6 7]

Transcriptome profiling and other advanced molecular biology approaches may provide detailed information on the dysfunctional cellular processes associated to complex pathologies[8] such as IPF. Indeed, various transcriptomic approaches have been successfully applied in recent years to different lung fibrosis models, mostly in mice, and to IPF in order to gain novel translationally relevant insights.[9–15] Only few studies have relied on rat lung fibrosis models, so far.[10 11] Furthermore, none of the previous rat studies employed a data-mining strategy to investigate time-dependent variations in transcriptional signatures to potentially gain more insights on the progression of BLM-induced lung damage. To fill this gap, we report here the results of a time-dependent integrated transcriptome and histomorphometric analysis performed in a rat double-hit BLM model of lung fibrosis up to 56 days postinduction. The main goal of this study was to assess the overlap in terms of dysregulated genes and pathways between the human disease, IPF and the animal model. In combination with previous results, the present work may provide a more robust starting point for the identification and prioritisation of new candidate targets as well as informative transcriptionally deregulated signatures to consider in the development of novel pharmacological treatments.

METHODS

A more detailed description can be found in online supplemental material.

Animals and BLM-induced lung fibrosis model

Male rats (Charles River, Italy) were intratracheally injected with BLM, 2 U/kg (BLM sulphate—Sigma, USA) or an equal volume of 0.9% saline solution (SAL) on day 0 and day 4, respectively. We used a single batch of BLM for all the treated animals, and we randomly assigned the BLM animals to have similar mean body weights among the different groups. We used the body condition score and Grimace Scale to monitor the overall health condition and to predict the actual establishment of the fibrotic lesions in the rat lungs. Rats were sacrificed on days 7, 14, 21, 28 and 56 (figure 1A). Moreover, a group of untreated animals (naïve) were sacrificed on day 0 for baseline condition assessments. Whole lungs were removed, and the right and left lobes were separated for the following analysis (figure 1A). After the terminal procedure, the whole lungs were removed, and right and left lobes were separated for following analysis. Left lung lobes of all eight animals of each group's time point were destined for histological analysis, while right lung lobes were randomly divided into two groups for different analytical procedures (homogenate for extraction of RNA or homogenate for evaluating some protein-based markers, details are in online supplemental materials.

Histopathology

To assess longitudinal fibrosis lesions, a score evaluation was made on formalin-fixed and paraffin-embedded left lung lobe stained slides, using a method based on the Ashcroft scale, as described previously[16] and modified by Hübner *et al*.[17] Stained slides were also scanned and acquired into the Visiopharm Integrator System (VIS; V.2017.2.4.3387) for a quantification of pulmonary fibrosis by automated analysis with the support of a VIS Analysis Protocol Package.

Transcriptomic analysis

RNA was extracted from right lungs using miRNeasy Mini Kit (QIAGEN, Netherlands), including DNase digestion protocol. Libraries for massive parallel RNA sequencing (RNA-seq) were prepared with the QuantSeq FWD (Lexogen) kit and sequenced with an Illumina NextSeq500 platform, which generated at least 30 million reads/sample (75 bp Single End). The dataset is available with accession number GSE212141. Differentially expressed genes (DEGs) between BLM and SAL samples were identified for each time point with the Limma-voom tool,[18] considering only genes with at least 10 counts in at least 3 samples. Genes were deemed as differentially expressed if the $\log_2$ fold-change (FC) was ≥1 or ≤−1 and the adjusted p≤0.05.

Modules of coexpressed genes between the different groups of treatment of all the time points were identified using the 'WeiGhted Correlation Network Analysis (WGCNA)' package in R.[19] Only genes with at least 10 counts in 22 samples out of 28 were kept for module construction (13 500 genes).

Gene set enrichment analysis (GSEA)[20] was used to compare the transcription profiles produced in this study with other published transcriptional signatures obtained in human IPF.[21–29] A leading-edge analysis was performed starting from the GSEA results of module 8 when compared with the human gene lists. From this analysis, we selected genes identified in at least 7/12 lists of upregulated or downregulated genes. The obtained gene list was subjected to GeneMANIA[30] online source and the network was visualised in Cytoscape[31] to highlight relevant information. The identification of significantly

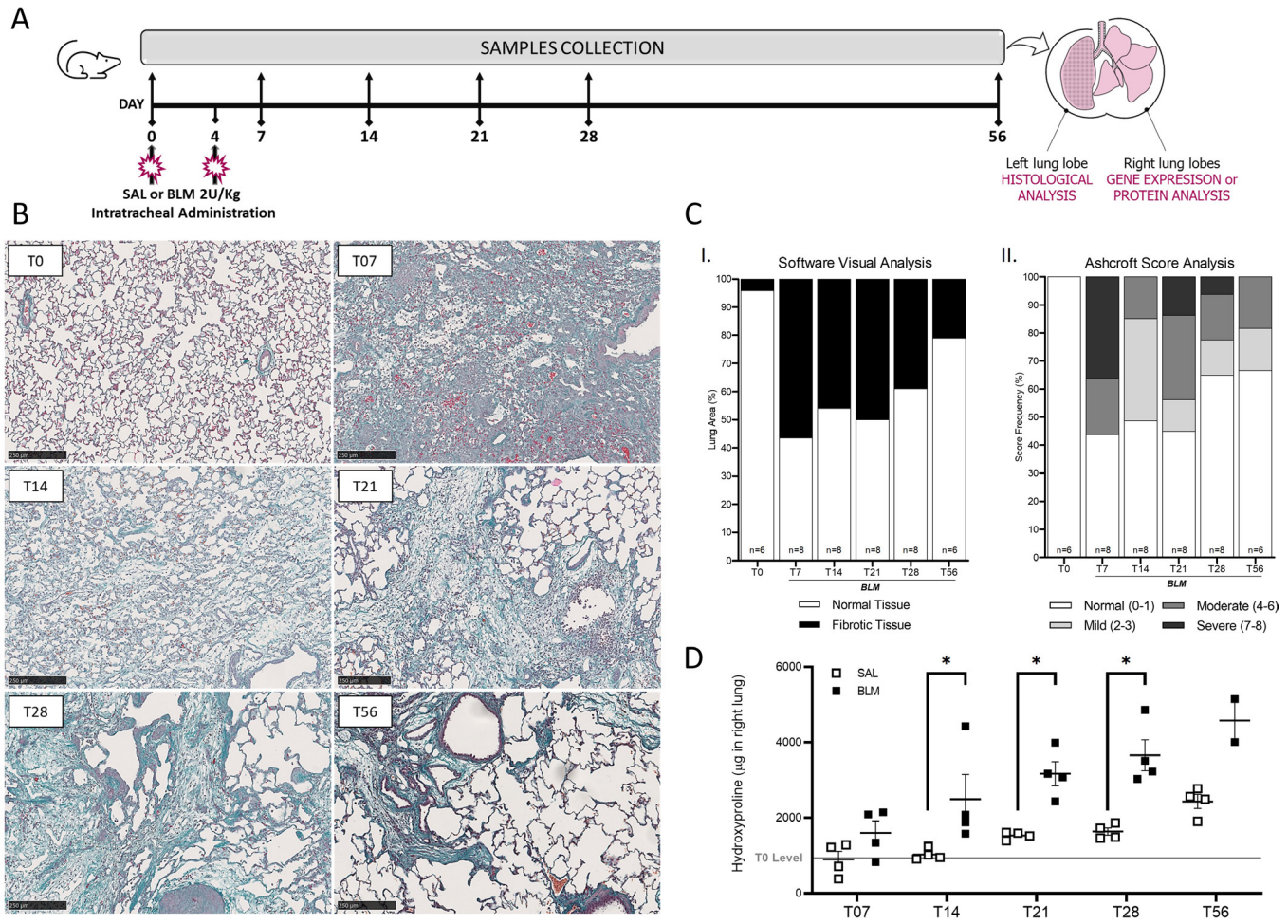

Figure 1 BLM-induced lung fibrosis in the rat. (A) Workflow and timeline of the experiment. At each time point, at least six animals per group were used. (B) Representative Masson's Trichrome-stained lung tissue sections at the starting point of the experiment (naïve animals, T0) and at 7, 14, 21, 28 and 56 days after the first BLM instillation. (C) Quantification of pulmonary fibrosis using the automated analysis (I) and Ashcroft Score evaluation (II) in BLM-treated and naïve animals. The mean values of % fibrosis and Ashcroft Score recorded in the BLM groups always significantly differed from the corresponding values measured in the SAL groups ($p \leq 0.05$). (D) Quantification of hydroxyproline level in lung homogenates obtained at the indicated time points from animals belonging to the SAL and BLM groups. The horizontal grey line represents the naïve (T0) level. The results were expressed as the mean±SEM; *$p<0.05$ BLM versus SAL. BLM, bleomycin; SAL, saline solution.

enriched pathways and processes was performed using Metascape.[32]

Hydroxyproline analysis in lung homogenate

Frozen right lobes were weighed and homogenised in 10 mL of ice-cold 1X PBS per g of tissue, with gentleMACS Dissociator (Miltenyi Biotec, Germany). The total amount of hydroxyproline was determined with the Hydroxyproline Colorimetric Assay Kit (Sigma MAK008, USA) according to the manufacturer's protocol.

Statistical analysis

The results were expressed as the mean±SEM. Mann-Whitney test calculations were made using GraphPad Prism V.8 (GraphPad Software, San Diego, California, USA) to examine differences between control animals (SAL) and the corresponding BLM-treated animals within the single time points. A $p<0.05$ was considered statistically significant.

RESULTS

Dynamic changes in histopathology and hydroxyproline content in the rat model of BLM-induced lung fibrosis

A comprehensive histological assessment was carried out at each time point (figure 1A–C). An acute and severe inflammation was clearly visible at day 7, with haemorrhage and alveolar infiltration by inflammatory cells and an initial diffuse matrix deposition around large blood vessels and bronchi.

Inflammation decreased at day 14, yet a diffuse matrix deposition persisted throughout the entire tissue sections. On day 21, large areas of lung parenchyma were replaced by a dense collagen deposition. A decreased severity, with a reduction of the total fibrotic area, was apparent at day

28. At day 56, a more prominent reduction of collagen accumulation was observed, with residual fibrotic areas thicker and denser than those observed at previous time points. All the above observations were confirmed by two semiquantitative analyses. On day 7, a fibrotic tissue area corresponding to approximately 55% of the total lung area was revealed by the Visual Analysis software (figure 1C.I). This value, which is nearly 10-fold higher than in the control samples (mean value: 5.8%) at all time points, remained almost unchanged till day 21 and gradually decreased thereafter. An analogous profile was confirmed by the Ashcroft score evaluation (figure 1C.II).

Hydroxyproline levels increased over time in the SAL group (figure 1D), likely reflecting a physiological collagen accumulation attributable to lung growth. However, a marked and significantly more sustained increase in hydroxyproline content was observed in the BLM group compared with the SAL group at each time point ($p<0.05$ at T14, T21 and T28).

Gene expression analysis revealed time-dependent transcriptional responses to BLM treatment

A total of 25 140 genes with above-background expression levels were revealed by RNAseq analysis. Principal component analysis (PCA) conducted on the whole transcriptome dataset (figure 2A) revealed coherent transcription profiles for the biological replicates, with a clear separation between the SAL group, which clustered close to the naïve group in the lower part of the PCA diagram, and BLM-treated animals in the mid-upper part of the diagram. A time-dependent variability and the observed distribution (from T07 to T56, left to right) is consistent with the increasing time interval after BLM administration. A time-dependent variability was observed in the SAL group, as well. Interestingly, the T07 SAL points

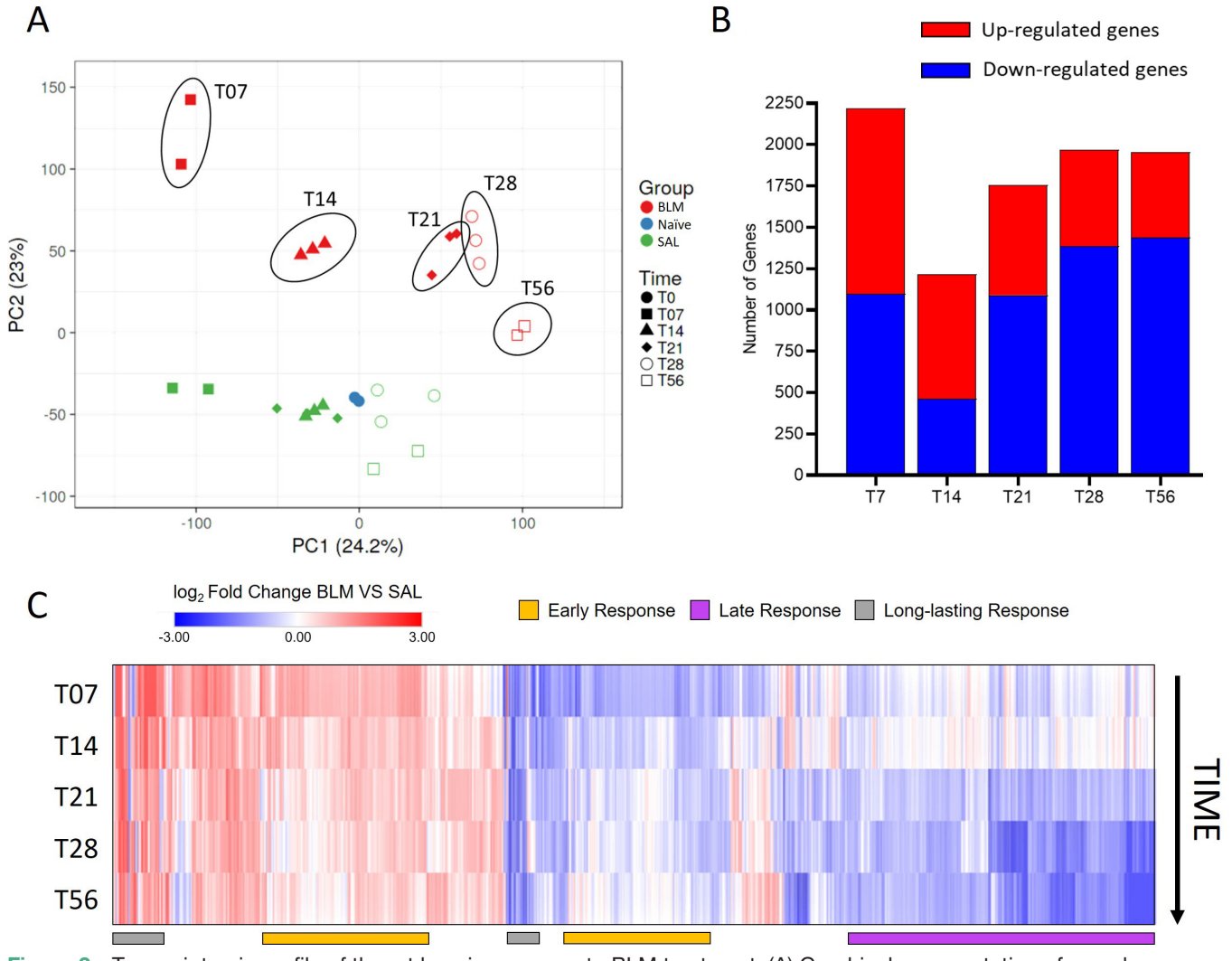

Figure 2 Transcriptomic profile of the rat lung in response to BLM treatment. (A) Graphical representation of sample distribution by PCA. (B) Bar graphs representing the number of upregulated and downregulated genes at each time point. (C) Heatmap of all genes deregulated in at least one time point. The hierarchical clustering of the columns was performed using a Euclidean distance metric. BLM, bleomycin; PCA, principal component analysis; SAL, saline solution.

were the most distant from the untreated condition, suggesting that the mere stress associated with intratracheal administration somehow contributes to transcriptome profile variability.

The number of DEGs identified at each time point ranged from 1217 (T14) to 2221 (T07), with a total of 4672 DEGs distributed across all the examined time points (figure 2B and online supplemental table S1). The number of upregulated genes exceeded the number of downregulated genes at T07 and T14, whereas the opposite trend was observed at later time points. As shown in the heatmap in figure 2C, DEGs followed a time-dependent pattern and exhibited rather specific expression trends. Based on hierarchical clustering, these were defined as 'early', 'late' and 'long-lasting' responses.

Identification of time-specific BLM-responsive gene sets using a network-based analysis

A network-based approach (WGCNA) was used to identify specific time-dependent transcriptional profiles and to convert the results of DEGs analysis into functionally relevant information. Unsigned WGCNA revealed 16 modules of coregulated (or antiregulated) genes. The first five modules accounted for 69.4% of all the analysed genes, while the remaining 11 modules contained less than 5% of genes each. The expression profiles of all individual Module Eigengenes (MEs) are reported in online supplemental figure S1 (see also online supplemental table S1 for detailed information on each gene). A pathway enrichment analysis was applied to the WGCNA modules to identify specific genes and pathways associated with the different time points. Figure 3A,B show the most informative modules and the most enriched pathways and processes comprised in each module. Indeed, modules 1–5 contain almost 70% of all the genes used for WGCNA, and module 8 is strongly correlated with both histological parameters. In agreement with the PCA, only a minimal variation was highlighted by the SAL versus naïve/T0 comparison. A much higher but internally consistent variation was, instead, revealed by BLM vs naïve/T0 and BLM versus SAL comparisons, which highlighted a predominant upregulation for modules 2, 8 and 5, and an opposite trend for all the remaining modules. Network analysis also allowed us to compare specific groups of coherently expressed genes with the phenotypic traits (eg, histopathological parameters) associated with each time point of the BLM treatment. As shown in figure 3A, two modules (3 and 8) significantly correlated with the Ashcroft Score and with the percentage of fibrosis derived from the same animals. Modules 8, 4 and 1 are truly representative of the three main types of responses that previously emerged in the DEGs analysis ('long-lasting', 'early' and 'late' responses, respectively; see also figure 2C). No appreciable gene expression variation was observed in SAL samples grouped in module 8, while a marked and persistent upregulation, starting from the earliest (T07) time point, was observed for the same module in BLM-treated samples. Module 8 was enriched in multiple extracellular matrix (ECM)-related pathways and positively correlated with histological parameters. Genes commonly associated with the fibrotic response, such as serpin family E member 1 (serpine1, alias plasminogen activator inhibitor 1(PAI1)), thrombospondin 2 (Thbs2), fibronectin 1 (Fn1) and matrix metallopeptidase 12 (Mmp12), whose expression variation was confirmed by independent validation approaches (see online supplemental figures S2 and S3), were strongly correlated to module 8. Module 4, intensely downregulated at early time points of BLM treatment, was enriched in pathways related to the circulatory system. Module 1 (>2500 genes) was largely unaffected by BLM treatment at T07 and T14 but displayed a marked downregulation at the last three time points. Based on this, quite peculiar expression profile and on the functional heterogeneity of the genes/pathways found to be enriched in module 1, ranging from kinase activity regulation to cell division/projection and chromatin modification, it is reasonable to hypothesise that the altered expression of this module is causally, although indirectly, related to the strong dysregulation observed in the early acute lung damage and tissue remodelling triggered by BLM.

Module 2 is characterised by an expression pattern very similar to that of module 8, with a clear trend towards upregulation at all the analysed time points. This module was enriched in cell cycle, cytoskeleton regulation and microtubules related pathways. Module 5 also displayed an expression pattern similar to that of module 8, even though the variation at T07 and T28 was not as marked as for the other time points. This was likely due to an increase in expression levels of the corresponding SAL time points with respect to T0, which reduced the statistical significance of most enrichment values except for the asparagine N-linked glycosylation and the endoplasmic reticulum to Golgi vesicle-mediated transport pathways. Module 3, instead, belongs to the late/long-lasting type of responses, with a marked and persistent downregulation becoming more prominent at the latest time points. Moreover, it is enriched in processes related to the leucocyte system, cell adhesion and cellular trafficking and was significantly anticorrelated with the histological parameters (Pearson correlation p value=5.0×10^{-12} and p value=1.2×10^{-7} for the Ashcroft Score and % Fibrosis, respectively).

Predictivity and translatability of the rat-BLM preclinical model to the human pathology

To evaluate the strength and overall consistency of the present transcriptome profiling data and to identify analogies between the animal model and human pathology, we used GSEA to compare our data with those retrieved from nine independent human IPF studies. In the ranked lists based on FC values obtained at different time points, GSEA revealed highly statistically significant NES values, especially in the case of IPF upregulated genes

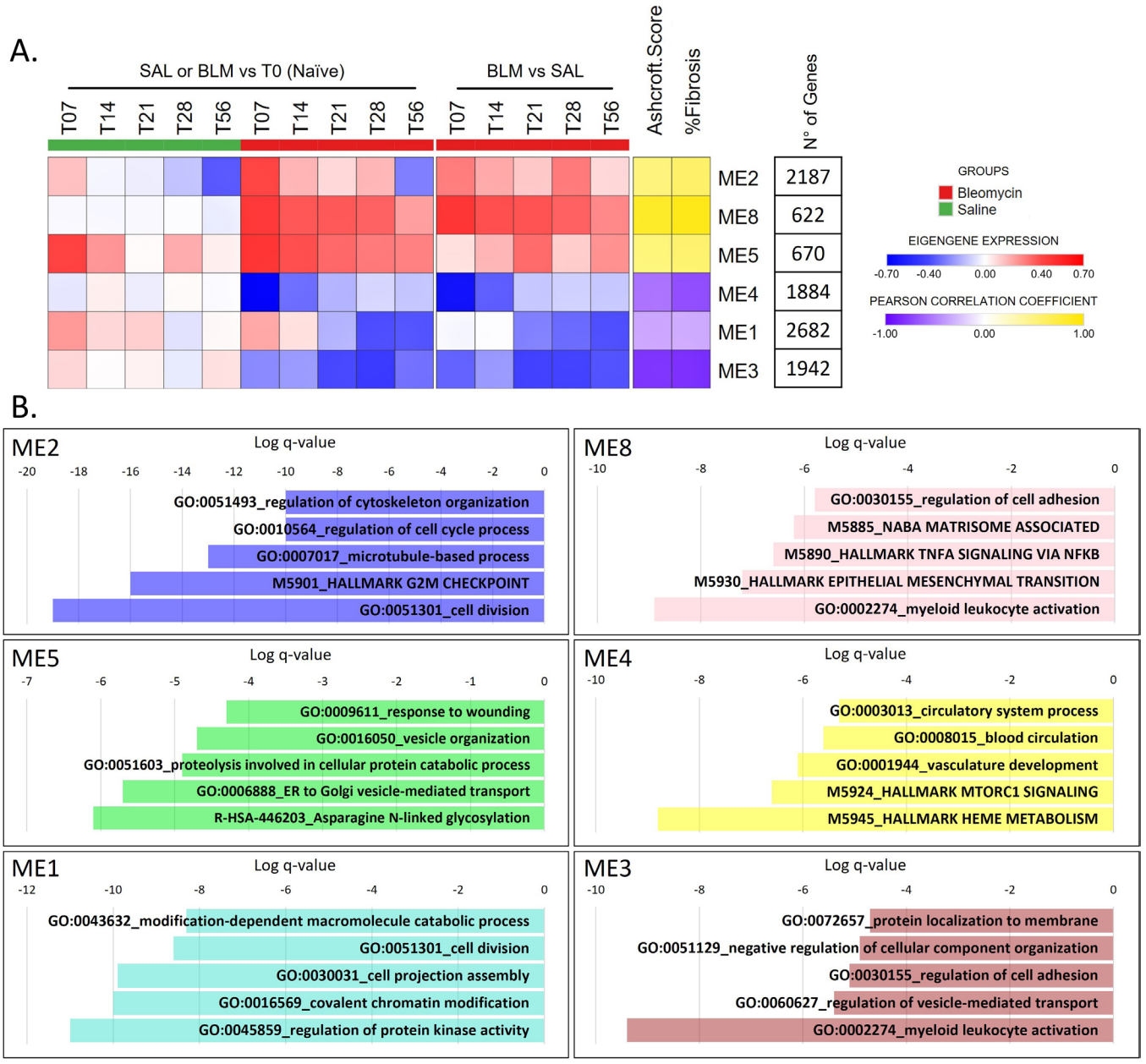

Figure 3 Time-dependent transcription profiles following BLM administration. (A) Heatmap of the most informative modules (represented by their module eigengene, MEs). Each square represents the eigengene expression of a single biological condition (column) in a specific ME (rows). The left part of the heatmap represents comparisons between SAL or BLM at each time point with T0 (log2 FC (SAL/T0) and log2 FC (BLM/T0), respectively), while the right part shows comparisons between SAL and BLM (log2 FC (BLM/SAL)), as reported above the columns label. The eigengene expression was calculated as the ratio between the average eigengene expression of the biological replicates and the eigengene expression of the control group of interest (T0 or respective SAL). The last two columns on the right show the Pearson correlation value between each ME and the two histological parameters. Only the correlation values of ME8 and ME3 were statistically significant (log p-val −6). (B) Bar graphs of the most enriched terms identified by Metascape of the modules shown in A. Bar graphs represent the Log q-values and indicate the most significant terms for each group of similar terms. See online supplemental figure 1 and table 1 for detailed information on all WGCNA modules. BLM, bleomycin; SAL, saline solution; WGCNA, weighted correlation network analysis.

(left part of figure 4). The highest NES values and overall concordance were observed for the ranked lists of the last three time points, which at the histological level were all characterised by pronounced ECM deposition. To better pinpoint the time-dependent gene signatures of the rat model that are more representative of the human disease, we ranked the list of genes based on the module membership values derived from the WGCNA (see online supplemental table S2). According to GSEA, module 8 is that with the highest and most significant NES values for nearly all the analysed human gene lists (figure 4), thus further emphasising the importance of the genes

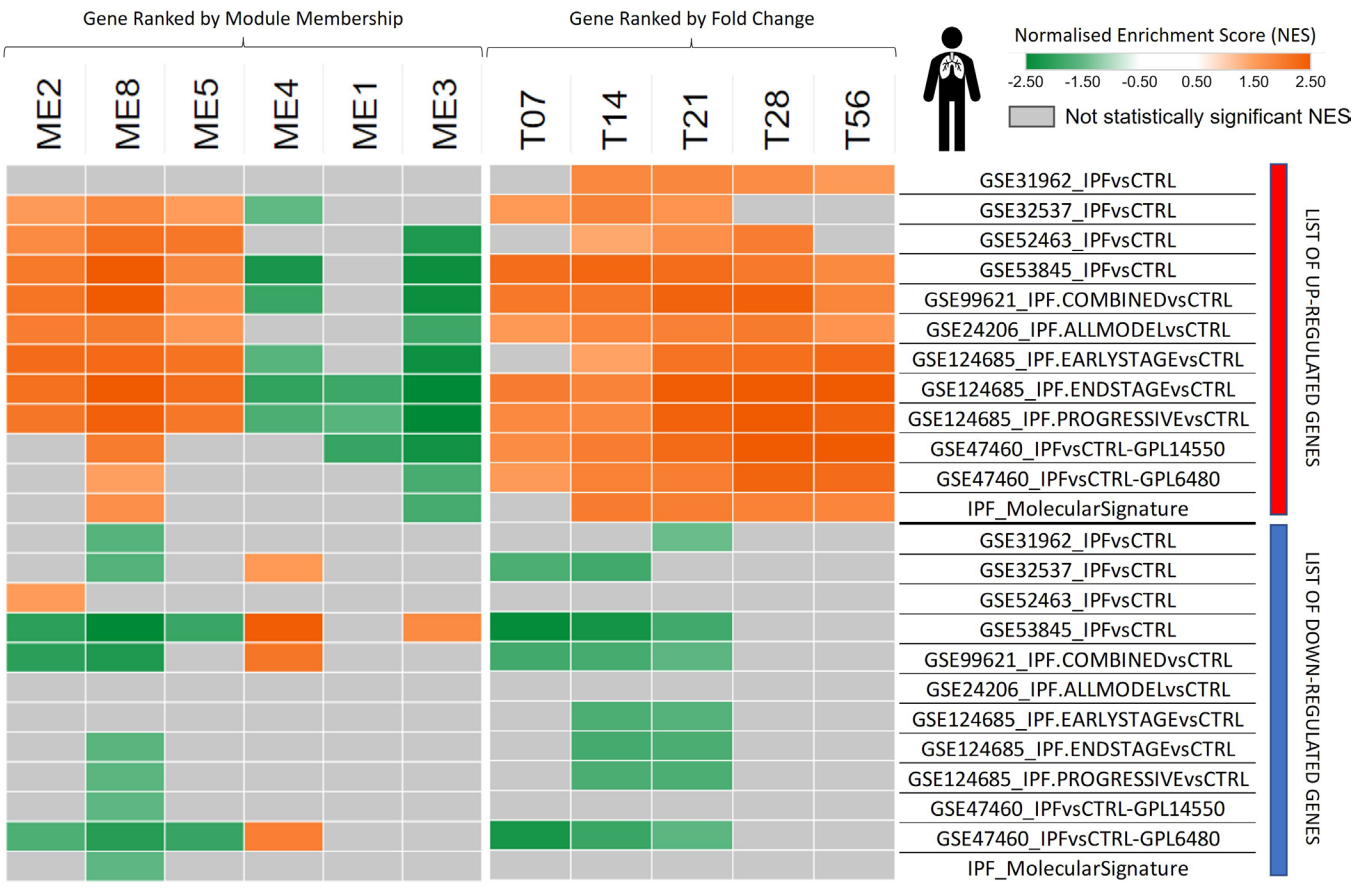

Figure 4 Association of gene signatures from time dependent BLM-induced rat lung with different human IPF samples detected by gene set enrichment analysis. The degree of enrichment of each analysed gene set (identified by the GEO accession number followed by a short description of the list) was determined against lists of preranked genes based on module membership (for the columns referred to the modules of the WGCNA on the left part of the image) or on log2 fold change (for the columns referred to the time points on the right part of the image). The NES is plotted in the heatmap with a scale form dark green (max negative NES) to dark orange (max positive NES). Grey: not significant NES (qval>0.05). BLM, bleomycin; IPF, idiopathic pulmonary fibrosis; WGCNA, weighted correlation network analysis.

included in this module. Significant NES values were also obtained for module 3, but at variance with module 8, these were restricted to the upregulated gene lists.

Considering the predictive potential of module 8 and its enrichment with IPF-related gene lists, we used the leading-edge analysis of GSEA to identify the most important and translationally relevant genes correlated to this module. This analysis led to the identification of a core set of genes that appear to be highly interlaced (figure 5). Interestingly, genes contained within this set mainly code for extracellular space and plasma membrane proteins, including key ECM components such as collagen type I (Col1a1) and type III (Col3a1) alpha 1.

DISCUSSION

Although the discovery of many new potential drug targets is aided by an in-depth knowledge of the human genome and multiomics approaches, the overall rate of new clinically approved drugs in IPF remains unsatisfactory. Recently, some drug candidates, proposed as highly promising treatments, have not met efficacy endpoints when evaluated in clinical trials, leaving unmet the urgent medical need for effective IPF therapies. The rate of success in drug development could arguably be increased by the availability of more clinically relevant animal models and stringent efficacy criteria during target validation and preclinical proof of concept establishment.

Animal models of IPF have provided valuable insights into the cellular and molecular mechanisms underlying the disease and have helped in identifying and testing multiple potential therapeutic interventions. Numerous models of IPF have been developed so far, including the use of chemical triggers such as BLM, monocrotaline, amiodarone, fluorescein isothiocyanate, oxidants and phorbol myristate acetate.[7] Other models rely on known aetiological agents including asbestos, silica and radiations[33] or on humanised murine models.[34–36] Epithelial cell dysfunction was postulated as an important component in the pathogenesis of IPF and animal models have been developed, accordingly. Indeed, telomere

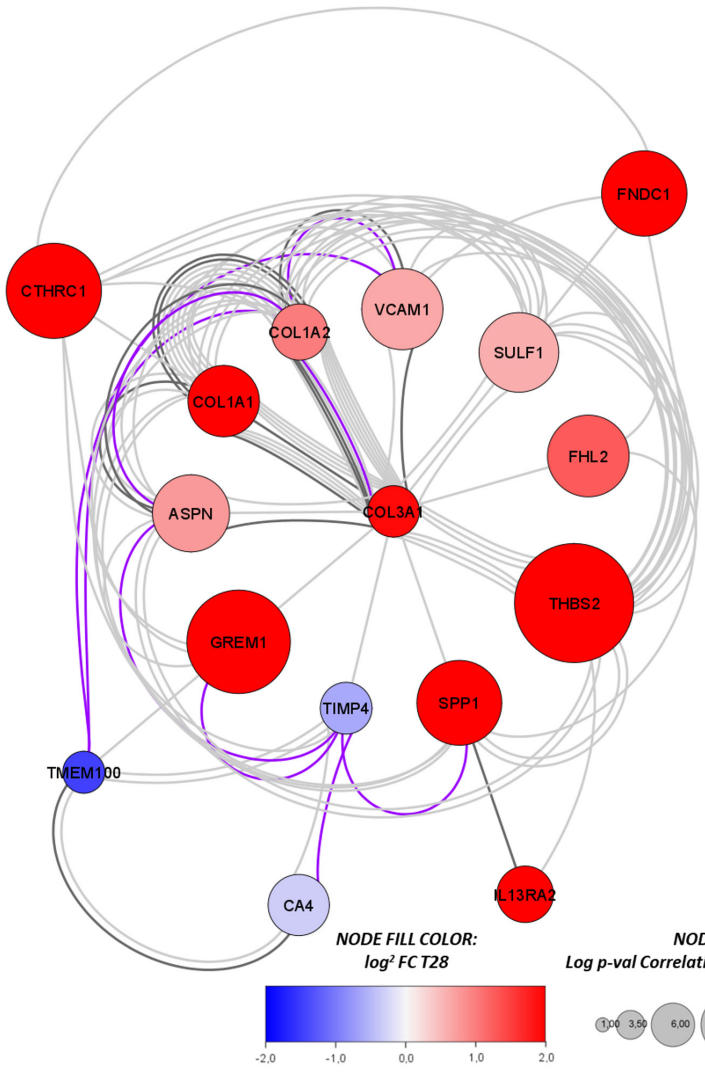

Gene Name	Gene Description	Location
COL1A1	collagen type I alpha 1 chain	Extracellular Space
COL1A2	collagen, type I, alpha 2	
COL3A1	collagen type III alpha 1 chain	
CTHRC1	collagen triple helix repeat containing 1	
GREM1	gremlin 1, DAN family BMP antagonist	
SPP1	secreted phosphoprotein 1	
THBS2	thrombospondin 2	
TIMP4	TIMP metallopeptidase inhibitor 4	
CA4	carbonic anhydrase 4	Plasma Membrane
FNDC1	fibronectin type III domain containing 1	
IL13RA2	interleukin 13 receptor subunit alpha 2	
TMEM100	transmembrane protein 100	
VCAM1	vascular cell adhesion molecule 1	
FHL2	four and a half LIM domains 2	Intracellular Space
ASPN	asporin	
SULF1	sulfatase 1	

Figure 5 Features of the most translationally relevant genes from module 8. Genes belonging to module 8, which are shared with the majority of human IPF studies (selected by GSEA leading edge analysis), are represented as a network to highlight their connections in terms of coexpression (light grey), colocalisation (dark grey) or genetic interaction (violet). Node size represents the correlation with the percentage of lung fibrosis; node colour represents the BLM induced (red) or repressed (blue) gene expression at T28. The table below gives a short gene description for each element of the figure. BLM, bleomycin; GSEA, gene set enrichment analysis; IPF, idiopathic pulmonary fibrosis.

dysfunction in type II AECs, mediated by deletion of the telomeric repeat binding factor 1, TRF1[37] and the expression of an IPF-associated SFTPC mutant in the pulmonary epithelium of mice in an allelic, inducible fashion,[38] were able to recapitulates some features of the human IPF phenotype. Adult Muc5b-deficient mice displayed bronchial hyperplasia and metaplasia, interstitial thickening, alveolar collapse, immune cell infiltrates, disorganised elastin fibres and collagen deposition.[39] Nevertheless, as also reported in the ATS workshop report, none of the currently known lung fibrosis animal models can fully recapitulate the complexity of IPF, and genetically modified animals, even if promising, may be better suited for discovery research than drug testing, so clinical candidates should be tested and validated for efficacy in more than one animal model/species.[6]

With this premise, we here report the first comprehensive gene-expression comparison between a time-course BLM model in the rat with the most recent gene-expression omic data coming from IPF patients. We used rats instead of mice for their slower development of the fibrotic lesions, for the different pulmonary architectures and tissue mechanical properties,[40 41] and for the focal aspects of fibroblast/myofibroblast agglomerates (unpublished findings). Development of pulmonary fibrosis induced by local administration of BLM in rodents is often unpredictable. There is a high degree of variability among individual animals in the extent of fibrosis, especially using batches of BLM developed for non-clinical use. With this respect, in this study, we used a single batch of BLM for all treated animals. Moreover, based on previous data collected over the time, we could

correlate the extent of lung fibrosis injury (histology and biomarker analysis) with a series of humane endpoints, like body weight. The weight loss and ponderal growth were comparable with a series of previous successful experiments conducted in the same laboratory.

In this study, we describe the time-dependent gene expression analysis transcriptome analysis over in a 56-day period of a rat model of lung fibrosis induced by a double administration of BLM. The lung whole transcriptome was flanked by a comprehensive histopathological assessment to gain a better understanding of the model in terms of translational potential and prospective utilisation for the discovery and functional selection of new IPF therapeutics. Importantly, a comparison of gene expression profiles between the rat model and IPF lung bulk datasets have been performed.

As already demonstrated for murine models, we confirmed that a double intratracheal instillation of BLM triggered an initially severe but transient inflammatory/fibrotic response, followed by a progressive fibrosis and ECM deposition, as revealed by the peak of hydroxyproline level measured at day 28. Histological parameters and hydroxyproline content at day 56 indicated a persistent fibrotic condition, although of reduced severity compared with earlier time points. The time-dependent response to BLM delineated by our analysis is in keeping with the results of previous preclinical studies[6 42 43] highlighting a switch from inflammation to fibrosis around the seventh day post-BLM treatment, followed by the appearance of fibrotic lesions starting from day 14 and a peak of collagen deposition at days 21–28. Preceding reports have indicated fibrosis resolution, with an almost complete recovery to a normal lung structure, within 4–8 weeks from BLM treatment,[6 44 45] but in this model, as well as in other time-course studies, no evidence of complete fibrotic resolution could be detected at day 56.[11 13 14 46] This finding suggests that lung fibrosis resolution requires more time in a model like this, so a larger therapeutic intervention window may be employed to assess the efficacy of drug candidates.

Transcriptomic analysis provided a detailed overview of BLM-induced pulmonary fibrosis development in the rat model. Three of the most informative modules of coregulated genes identified by WGCNA represent specific and mechanistically relevant time-related responses to BLM. Previously, Peng *et al*[13] reported the existence of distinct time-specific gene expression responses to BLM in a mouse model of lung fibrosis. Using hierarchical clustering analysis, they identified an inflammatory phase (days 1–2), an active fibrosis phase (days 7–14) and a late fibrosis phase (days 21–35), with no evidence of an enduring temporal response. In our model, the 'long-lasting' response, enclosed in module 8, undoubtedly provided the most characteristic representation of the fibrotic condition. In fact, this module strongly correlated with histological parameters and comprised several genes frequently associated with fibrotic diseases, including Serpine1, Thbs2, Fn1 and Mmp12. Importantly, despite the challenges due to the heterogeneity of the human disease and the IPF lung itself, as well as the high variability between studies,[29] module 8 displayed the best correlation with almost all transcriptomic profiles previously documented on IPF patients.[21–29] The pathways associated with the 'long-lasting' response suggest a collaborative role of myeloid lineage cells and multiple pathways associated with ECM composition and modulation. Although it is generally accepted that IPF is not primarily caused by an immunopathogenic process, animal models and human research studies have shown that immune cells play a significant and varied role in disease development and can regulate fibrotic responses.[47] In this regard, the observation that interleukin 13 receptor subunit alpha 2 (IL13Rα2) is among the genetically interacting pathways shared by BLM rat lung and human IPF (figure 5), supports potential immune-mediated mechanisms underlying ILDs.[25]

The occurrence of a reparative response at day 56, as confirmed by histological analysis, is unquestionably a distinguishing feature of the animal model compared with IPF. The contrast between this 'reversible' condition and the progressive and irreversible nature of IPF could explain why there was only a weak link between the late transcriptional response indicated by module 1 and human studies. However, some insight could be gained from the examination of this response, which might provide important informative clues on the resolution of lung fibrosis. A future, more detailed understanding of this late response, which is specifically present in our model in comparison to others (see online supplemental figure S4), may allow us to pinpoint the underlying mechanisms that, by promoting lung tissue repair, may uncover new therapeutic targets of fibrotic conditions. Given the histological data and the suitable correlation of genes modulated in our model with the gene expression profile of IPF patients, this model could be used to assess the antifibrotic potential of a drug acting on a time frame that is durable enough to be reliably monitored over a 3-week treatment window (from day 7 to day 28). Furthermore, because some of the genes associated with the 'long-lasting' response are translationally relevant, combining histological parameters with specific gene expression signatures as a functional readout could be useful in drug discovery/target validation experiments for a more reliable, human disease-oriented assessment of novel pharmacological treatments. Similar contentions cannot be applied to other models based on a single administration of BLM in spite of a broad overlap between the models. Indeed, the effect on the core of our identified gene set is generally low or not statistically significant (see online supplemental figure S5), particularly at T28, as shown by the GSEA analysis (see online supplemental figure S4 and table S3).

In conclusion, despite the limitations described above and the ambiguous clinical relevance of the selected rodent model to mimic IPF, we proposed a comprehensive gene-expression cross-comparison between a temporal evolution of lung fibrosis induced by two

sequential intratracheal administrations of BLM in rats and nine different human IPF studies. A key finding of the present analysis is the identification of a group of dysregulated genes, mostly related to ECM homoeostasis, which are shared by the animal model and the human disease. Thus, this model may be particularly valuable for the screening and preclinical efficacy evaluation of new potential therapeutics acting on aberrant ECM tissue deposition.

Author affiliations
[1]Department of Chemistry Life Sciences and Environmental Sustainability, University of Parma, Parma, Italy
[2]Department of Medicine Solna (MedS) and Center for Molecular Medicine (CMM), Karolinska Institutet, Solna, Sweden
[3]Corporate Preclinical R&D, Chiesi Farmaceutici SpA, Parma, Italy
[4]Department of Medicine and Surgery, University of Parma, Parma, Italy
[5]DKFZ - German Cancer Research Center, Heidelberg, Germany
[6]Interdepartmental Research Centre Biopharmanet-Tec, University of Parma, Parma, Italy

Acknowledgements This manuscript is based on the original research conducted by Martina Bonatti in her PhD thesis titled 'Biomolecular characterisation of a rat model of lung fibrosis: investigation of its translational potential in Idiopathic Pulmonary Fibrosis (IPF)'.

Contributors Study design: VP, SO, BM and MT. Performance of the experiments: MB, VP, PC, SP and MGP. Data acquisition: MB, VP, PC, SP, MGP, CF, CM and BM. Data analysis: MB, VP, SC and BM. Manuscript drafting: MB. Interpretation of the results and manuscript revision: MB, VP, PC, SP, MGP, CF, CM, CAML, FQ, SC, SO, GV, MC, BM and MT. BM and MT are guarantors for the manuscript.

Funding This work was supported by Chiesi Farmaceutici S.p.A., no grant number awarded.

Competing interests VP, PC, SP, MGP, CM, GV, MC and MT are employees of Chiesi Farmaceutici S.p.A. FQ was engaged as consultant by Chiesi Farmaceutici S.p.A. All the remaining Authors have not actual and perceived conflicts of interest.

Patient and public involvement Patients and/or the public were not involved in the design, or conduct, or reporting, or dissemination plans of this research.

Patient consent for publication Not applicable.

Ethics approval All the procedures involving animals were reviewed, approved and authorised by (1) The Italian Public Health System for Animal Health and Food Safety within the Italian Ministry of Health (MoH)(authorisation number 1066/2015-PR) and by (2) the Chiesi Body for the Protection of Animals (OPBA) committee. All the procedures were performed within a certified animal facility: AAALAC (American Association for Accreditation of Laboratory Animal Care, https://www.aaalac.org/). Experiments were performed in full compliance with the European ethics standards in conformity with directive 2010/63/EU, Italian D. Lgs 26/2014, the revised 'Guide for the Care and Use of Laboratory Animals' (Guide for the Care and Use of Laboratory Animals, 1996), and the ARRIVEguidelines (Animal Research: Reporting of In Vivo Experiments). Human data used in this study were taken from published datasets.

Provenance and peer review Not commissioned; externally peer reviewed.

Data availability statement Data are available in a public, open access repository. The dataset is available in the Gene Expression Omnibus data repository (https://www.ncbi.nlm.nih.gov/geo/) with accession number GSE212141.

ORCID iDs
Martina Bonatti http://orcid.org/0000-0003-3183-6831
Barbara Montanini http://orcid.org/0000-0002-5419-7975

REFERENCES

1 Lee AS, Mira-Avendano I, Ryu JH, *et al*. The burden of idiopathic pulmonary fibrosis: an unmet public health need. *Respir Med* 2014;108:955–67.
2 Raghu G, Collard HR, Egan JJ, *et al*. An official ATS/ERS/JRS/ALAT statement: idiopathic pulmonary fibrosis: evidence-based guidelines for diagnosis and management. *Am J Respir Crit Care Med* 2011;183:788–824.
3 Poletti V, Ravaglia C, Tomassetti S. Pirfenidone for the treatment of idiopathic pulmonary fibrosis. *Expert Rev Respir Med* 2014;8:539–45.
4 Rogliani P, Calzetta L, Cavalli F, *et al*. Pirfenidone, nintedanib and N-Acetylcysteine for the treatment of idiopathic pulmonary fibrosis: a systematic review and meta-analysis. *Pulm Pharmacol Ther* 2016;40:95–103.
5 Tomioka H, Takata H. Treatment with nintedanib for acute exacerbation of idiopathic pulmonary fibrosis. *Respirol Case Rep* 2017;5:e00215.
6 Jenkins RG, Moore BB, Chambers RC, *et al*. An official American thoracic society workshop report: use of animal models for the preclinical assessment of potential therapies for pulmonary fibrosis. *Am J Respir Cell Mol Biol* 2017;56:667–79.
7 Tashiro J, Rubio GA, Limper AH, *et al*. Exploring animal models that resemble idiopathic pulmonary fibrosis. *Front Med (Lausanne)* 2017;4:118.
8 Casamassimi A, Federico A, Rienzo M, *et al*. Transcriptome profiling in human diseases: new advances and perspectives. *Int J Mol Sci* 2017;18:1652.
9 Vukmirovic M, Kaminski N. Impact of transcriptomics on our understanding of pulmonary fibrosis. *Front Med (Lausanne)* 2018;5:87.
10 Park H-J, Yang M-J, Oh J-H, *et al*. Genome-wide transcriptional response during the development of Bleomycin-induced pulmonary fibrosis in Sprague-Dawley rats. *Toxicol Res* 2010;26:137–47.
11 Bauer Y, Tedrow J, de Bernard S, *et al*. A novel genomic signature with translational significance for human idiopathic pulmonary fibrosis. *Am J Respir Cell Mol Biol* 2015;52:217–31.
12 Shichino S, Ueha S, Hashimoto S, *et al*. Transcriptome network analysis identifies protective role of the LXR/SREBP-1C axis in murine pulmonary fibrosis. *JCI Insight* 2019;4:e122163.
13 Peng R, Sridhar S, Tyagi G, *et al*. Bleomycin induces molecular changes directly relevant to idiopathic pulmonary fibrosis: a model for 'active' disease. *PLoS One* 2013;8:e59348.
14 Cabrera S, Selman M, Lonzano-Bolaños A, *et al*. Gene expression profiles reveal molecular mechanisms involved in the progression and resolution of bleomycin-induced lung fibrosis. *Am J Physiol Lung Cell Mol Physiol* 2013;304:L593–601.
15 Kaminski N, Allard JD, Pittet JF, *et al*. Global analysis of gene expression in pulmonary fibrosis reveals distinct programs regulating lung inflammation and fibrosis. *Proc Natl Acad Sci U S A* 2000;97:1778–83.
16 Ashcroft T, Simpson JM, Timbrell V. Simple method of estimating severity of pulmonary fibrosis on a numerical scale. *J Clin Pathol* 1988;41:467–70.
17 Hübner R-H, Gitter W, El Mokhtari NE, *et al*. Standardized quantification of pulmonary fibrosis in histological samples. *Biotechniques* 2008;44:507–11,
18 Ritchie ME, Phipson B, Wu D, *et al*. Limma powers differential expression analyses for RNA-sequencing and Microarray studies. *Nucleic Acids Res* 2015;43:e47.
19 Langfelder P, Horvath S. WGCNA: an R package for weighted correlation network analysis. *BMC Bioinformatics* 2008;9:559.
20 Subramanian A, Kuehn H, Gould J, *et al*. GSEA-P: a desktop application for gene set enrichment analysis. *Bioinformatics* 2007;23:3251–3.
21 McDonough JE, Ahangari F, Li Q, *et al*. Transcriptional regulatory model of fibrosis progression in the human lung. *JCI Insight* 2019;4:e131597.
22 DePianto DJ, Chandriani S, Abbas AR, *et al*. Heterogeneous gene expression signatures correspond to distinct lung pathologies and biomarkers of disease severity in idiopathic pulmonary fibrosis. *Thorax* 2015;70:48–56.
23 Meltzer EB, Barry WT, D'Amico TA, *et al*. Bayesian probit regression model for the diagnosis of pulmonary fibrosis: proof-of-principle. *BMC Med Genomics* 2011;4:70.

24 Yang IV, Coldren CD, Leach SM, *et al*. Expression of Cilium-associated genes defines novel molecular subtypes of idiopathic pulmonary fibrosis. *Thorax* 2013;68:1114–21.
25 Luzina IG, Salcedo MV, Rojas-Peña ML, *et al*. Transcriptomic evidence of immune activation in macroscopically normal-appearing and scarred lung tissues in idiopathic pulmonary fibrosis. *Cell Immunol* 2018;325:1–13.
26 Steele MP, Luna LG, Coldren CD, *et al*. Relationship between gene expression and lung function in idiopathic interstitial pneumonias. *BMC Genomics* 2015;16:869.
27 Yang IV, Burch LH, Steele MP, *et al*. Gene expression profiling of familial and sporadic interstitial pneumonia. *Am J Respir Crit Care Med* 2007;175:45–54.
28 Nance T, Smith KS, Anaya V, *et al*. Transcriptome analysis reveals differential splicing events in IPF lung tissue. *PLoS One* 2014;9:e97550.
29 Gangwar I, Kumar Sharma N, Panzade G, *et al*. Detecting the molecular system signatures of idiopathic pulmonary fibrosis through integrated genomic analysis. *Sci Rep* 2017;7:1554.
30 Warde-Farley D, Donaldson SL, Comes O, *et al*. The genemania prediction server: biological network integration for gene prioritization and predicting gene function. *Nucleic Acids Res* 2010;38:W214–20.
31 Shannon P, Markiel A, Ozier O, *et al*. Cytoscape: a software environment for integrated models of Biomolecular interaction networks. *Genome Res* 2003;13:2498–504.
32 Zhou Y, Zhou B, Pache L, *et al*. Metascape provides a biologist-oriented resource for the analysis of systems-level datasets. *Nat Commun* 2019;10.
33 Miles T, Hoyne GF, Knight DA, *et al*. The contribution of animal models to understanding the role of the immune system in human idiopathic pulmonary fibrosis. *Clin Transl Immunology* 2020;9:e1153.
34 Pierce EM, Carpenter K, Jakubzick C, *et al*. Therapeutic targeting of CC ligand 21 or CC Chemokine receptor 7 Abrogates pulmonary fibrosis induced by the adoptive transfer of human pulmonary fibroblasts to immunodeficient mice. *Am J Pathol* 2007;170:1152–64.
35 Trujillo G, Meneghin A, Flaherty KR, *et al*. TLR9 differentiates rapidly from slowly progressing forms of idiopathic pulmonary fibrosis. *Sci Transl Med* 2010;2:57ra82.
36 Fujii H, Luo Z-J, Kim HJ, *et al*. Humanized chronic graft-versus-host disease in NOD-SCID Il2Rgamma-/- (NSG) mice with G-CSF-mobilized peripheral blood mononuclear cells following cyclophosphamide and total body irradiation. *PLoS One* 2015;10:e0133216.
37 Naikawadi RP, Disayabutr S, Mallavia B, *et al*. Telomere dysfunction in alveolar epithelial cells causes lung remodeling and fibrosis. *JCI Insight* 2016;1:e86704.
38 Nureki S-I, Tomer Y, Venosa A, *et al*. Expression of mutant Sftpc in murine alveolar epithelia drives spontaneous lung fibrosis. *J Clin Invest* 2018;128:4008–24.
39 Valque H, Gouyer V, Duez C, *et al*. Muc5B-deficient mice develop early histological lung abnormalities. *Biol Open* 2019;8:bio046359.
40 Faffe DS, Rocco PRM, Negri EM, *et al*. Comparison of rat and mouse pulmonary tissue mechanical properties and histology. *J Appl Physiol (1985)* 2002;92:230–4.
41 Treuting PM, Treuting PM, Dintzis SM, *et al*. *Comparative anatomy and histology: a mouse, rat and human atlas, 2nd ed*. London, England: Academic Press, 2018.
42 Yanagihara T, Chong SG, Vierhout M, *et al*. Current models of pulmonary fibrosis for future drug discovery efforts. *Expert Opin Drug Discov* 2020;15:931–41.
43 Chaudhary NI, Schnapp A, Park JE. Pharmacologic differentiation of inflammation and fibrosis in the rat Bleomycin model. *Am J Respir Crit Care Med* 2006;173:769–76.
44 Schiller HB, Fernandez IE, Burgstaller G, *et al*. Time- and compartment-resolved proteome profiling of the extracellular niche in lung injury and repair. *Mol Syst Biol* 2015;11:819.
45 Moore BB, Hogaboam CM. Murine models of pulmonary fibrosis. *Am J Physiol Lung Cell Mol Physiol* 2008;294:L152–60.
46 Robbe A, Tassin A, Carpentier J, *et al*. Intratracheal Bleomycin Aerosolization: the best route of administration for a scalable and homogeneous pulmonary fibrosis rat model *Biomed Res Int* 2015;2015:198418.
47 Desai O, Winkler J, Minasyan M, *et al*. The role of immune and inflammatory cells in idiopathic pulmonary fibrosis. *Front Med (Lausanne)* 2018;5:43.